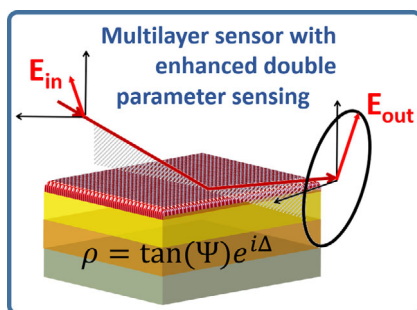


RESEARCH ARTICLES

I. Aulika,* M. Zubkins, J. Butikova,
J. Purans 2100424

**Enhanced Reflectivity Change and Phase
Shift of Polarized Light: Double
Parameter Multilayer Sensor**



Multilayer sensor shows great sensitivity to thickness and refractive index variation of the detectable material by measuring the reflectivity ratio Ψ and phase shift Δ . Focus is on a new biomedical sensor development, which has sensitivity to both parameters (Ψ , Δ) in the visible spectral range, thus opening the possibility for further research on enhanced double parameter sensing.

Enhanced Reflectivity Change and Phase Shift of Polarized Light: Double Parameter Multilayer Sensor

Ilze Aulika,* Martins Zubkins, Jelena Butikova, and Juris Purans

Herein, the concept of point of darkness based on polarized light phase difference and absorption of light is demonstrated by simulations using low refractive index and extinction coefficient semiconductor and dielectric, and high refractive index nonoxidizing metal multilayer thin film structures. Several multilayer sensor configurations show great sensitivity to thickness and refractive index variation of the detectable material by measuring the reflectivity ratio Ψ and phase shift Δ . Focus is on such multilayers, which have sensitivity to both parameters (Ψ , Δ) in the visible spectral range, thus opening the possibility for further research on a new biomedical sensor development with enhanced double parameter sensing.

1. Introduction

Biomedical sensor development for healthcare and diagnostics is a very rapidly growing market, which was valued at USD 22.4 billion in 2020 and is expected to expand at a compound annual growth rate (CAGR) of 7.9% from 2021 to 2028.^[1] In general, there are two types of biosensors, sensor patch and embedded devices, which use different detection mechanisms, e.g., electrochemical, optical, piezoelectric, thermal, and nanomechanical biosensors. Among all these technologies, the optical sensors have several advantages in the number of different receptor types and, moreover, permit the integration of different sensing mechanisms. Recent and very elaborated review (covering nearly 250 research articles) about optical biomedical sensors based on surface plasmon resonance (SPR), evanescent wave fluorescence, reflectometric (sometimes called also refractive), bioluminescence, and several others showed the huge potential for the broad use of these sensors in point-of-care testing devices and early-stage disease prediction.^[2]

Reflectometric biosensors^[3] are very attractive because they are relatively simple with respect to SPR and other methods, they are very sensitive, time-resolved, and label-free techniques. Under reflectometric principle of biosensing we can find such methods as reflectometric interference spectroscopy,^[4] interferometric reflectance imaging,^[5] and spectroscopic ellipsometry^[6] (SE), where the main sensing response is to a slight change in

layer thickness d seen as a shift of the interference pattern within the wavelength domain. The analyte concentration is determined by variations in the amplitude and phase of polarized light due to changes in the refractive index n and thickness of an adsorbed layer of the analyte^[1,4–6] (Figure 1).

1.1. SE


SE is a very powerful method for sensing very thin layers. Many of the commercially available SE instruments measure the main ellipsometric angles (Ψ , Δ) with 0.001° resolution, thus SE can measure the subangstrom thickness change^[7] and can detect the presence of very small amount of substances. For example, experimentally, it was reported detection limits of immunoglobulin G (IgG) 15, 0.1 ng mL⁻¹ of hepatitis B surface antigen, 0.01 ng mL⁻¹ α -fetoprotein, and 10 amol mL⁻¹ in DNA-hybridization studies.^[6–10] SE has been demonstrated to be a very promising sensor.^[6–10] There are first signs toward miniaturization of SE and SPR^[11–13], and active research on metasurfaces for applications as active optical components^[14] in miniature optical sensor and devices. It is expected that the optical biosensor development and market share with respect to other biosensor technologies is going to increase very rapidly in the nearest decades.^[1,2,15]

In ellipsometry, the two main ellipsometric angles (Ψ , Δ), functions of wavelength λ and incident angle of light θ , are defined by

$$\rho \equiv \tan(\Psi)e^{i\Delta} = \frac{|\tilde{r}_p|}{|\tilde{r}_s|} = \frac{E_p^{\text{out}}/E_p^{\text{in}}}{E_s^{\text{out}}/E_s^{\text{in}}} \quad (1)$$

where \tilde{r}_p and \tilde{r}_s are Fresnel's coefficients for p (parallel) and s (perpendicular) polarized light; E_p^{out} , E_p^{in} , E_s^{out} , and E_s^{in} represent p and s components of the incident and reflected electric fields of the light beam.^[16] $\tan\Psi$ is the amplitude ratio upon reflection and $\Delta = \delta_p - \delta_s$ is the phase shift induced by the reflection between the p -wave and the s -wave. The ratio ρ is related to the optical properties of the material or materials under investigation, namely, the complex refractive index $\tilde{N} = n + ik$, where n is the index of refraction and k is the extinction coefficient. The high sensitivity of this technique is derived from the fact that the measured (Ψ , Δ) is a relative measurement of the change in polarization (a ratio or difference of two values rather than the absolute value of either). It explains robustness, the high accuracy, and the reproducibility of the technique.

I. Aulika, M. Zubkins, J. Butikova, J. Purans
Institute of Solid State Physics
University of Latvia (ISSP UL)
LV-1063 Riga, Latvia
E-mail: ilze.aulika@cfi.lu.lv

 The ORCID identification number(s) for the author(s) of this article can be found under <https://doi.org/10.1002/pssa.202100424>.

DOI: 10.1002/pssa.202100424

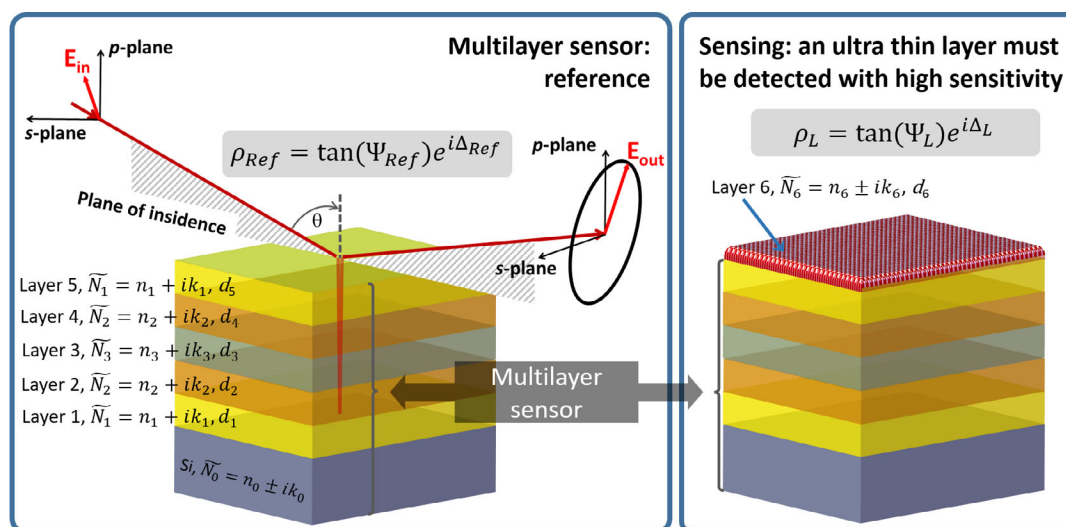


Figure 1. Schematic illustration of the sensory device based on reflectivity measurement setup with the capability to measure the ratio of the amplitude and the phase shift.

1.2. Other Aspects of Reflectance Methods

Exploiting further the reflectance methods for biomedical sensor applications such as SPR, reflectance, and transmittance, it is important to develop such sensors which have high surface sensitivity: when any material of very low thickness (≈ 0.1 nm) or of very small amount with different (n, k) values (with respect to the sensor) is present on the surface of the sensor, it is detected by measuring reflectance, transmittance, phase shift, wavelength, or incident angle shift. In the recent years much attention has been paid to the point of darkness^[17,18,20] based on perfect absorption of light and phase singularity. The absence of reflection can be achieved at the Brewster angle θ_B . Such suspension of the reflected light can be achieved in particular cases: ideal optical systems, prism-coupled SPR, the light reflection from a single interface,^[6] coherent absorption, and parity-time metamaterial. Different subwavelength nanostructures also have been proposed for the realization of topological darkness.^[17,19] Recently, it was reported on dispersion topological darkness at multiple wavelengths and polarization states using a three-layered structure where the top layer was nanopatterned.^[19] Also, simpler systems were reported, where the point of darkness is achieved by the multistack made of, e.g., Ag (20 nm)/methyl methacrylate MMA (522 nm)/Ge (10 nm) Ag⁻¹ (80 nm).^[20] For our knowledge, there are relatively many publications for multilayer structures with the point of darkness at NIR and IR wavelength range,^[19–25] and just few related to visible spectra range.^[25,26] The reason is that the high efficiency absorption (at specific λ) is mainly caused by the Fabry–Perot resonance in the non-absorbing dielectric layer placed in the middle of the stack: that results in trapping of the resonant light in dielectric layer and thus in enhancement of absorption efficiency. The light trapping (multiple internal light reflecting) is provided by materials with high (n, k) values below and on the top of dielectric layer. This system can be imagined also as a kind of light guide where the internal layer has n values lower with respect to the outer layer's n values.

In case of prototyping of systems with point of darkness, the complete suppression of reflection is practically not possible due to sensor fabrication errors (disorder, inhomogeneity, thickness variation, etc.), complex nanopatterning processes for metamaterial fabrication, natural oxidation of some metal layers, and polymer layer degradation under humidity and UV light. Interestingly, in case of multilayer stacks there are many studies devoted for the zero reflection (or perfect absorption), but not so many are dealing with the phase singularities and shifts. Probably it is related to the fact that it is easy to develop and do numerical simulation for the perfect absorption of light using, e.g., Fabry–Perot resonances or SPR approach, but both zero reflection and the phase sensitive sensors are a challenge. Phase-sensitive optical biosensing is of great importance in the development of single molecule and low concentration solution studies.^[2,6,17,18,20] The SPR approach, where the key parameters are the shift in the wavelength and/or incident angle, is extensively studied,^[14,17,18,28–34] while change in reflectivity and phase shift is relatively less studied.^[6,17,18,20] Some phase sensitive sensor systems are shown in **Table 1**, comparing technologically more challenging sensors with sensors fabricated with the simpler processes.

One possibility to achieve both (reflectivity and phase sensitivity) is by introducing into the multilayer stack a highly absorbing ultrathin layer, e.g., Ge.^[19,20,27] In this work, we propose an alternative: very thin multilayer system made of five films containing semiconductor and dielectric materials with low (n, k) . By varying the thickness of the films and choosing semiconductors with lower refractive index with respect to Ge material, and combining them with dielectrics and metals in a multilayer stack, it is possible to obtain relatively broad spectral range for point of darkness, thus “adjusting” the sensor design to the easier, custom, more convenient, or cheaper prototyping. This complementary approach offers a possibility to develop new and sustainable biomedical sensors, which can

Table 1. Some phase sensitive sensor description, fabrication technology, spectral range or λ and indented angle of light θ of work, detected material during sensor test, and measured parameters (difference of the main SE angles $d\Psi$ and $d\Delta$).

| Sensor description | Fabrication technology | Spectral range [nm] | Detected material | Parameter | References |
|---|---|--|---|---|------------|
| Plasmonic metamaterial; topologically protected darkness | | | | | |
| SE of Au array with the graphene: average size of the dots 110 nm, separation 140 nm | High complexity: • e-beam lithography • e-beam evaporation • wet-etching • micromini | Point of darkness at: • $\lambda = 603$ nm • $\theta \approx 69^\circ$ | Graphene hydrogenation; mass sensitivity < 10 fgmm ⁻² | $d\Psi = 34^\circ$ $d\Delta = 44^\circ$ | [17] |
| SE of Au array with the graphene: average size of the dots 135 nm, separation 140 nm | • surface functionalization | Point of darkness at: • $\lambda = 710$ nm • $\theta \approx 53^\circ$ | 10 pM streptavidin solutions in 10 mM phosphate-buffered; sensitivity 1–4 molecules per nanodot | $d\Psi = 25^\circ$ $d\Delta = 25^\circ$ | |
| Spectrometer and fringe pattern (for relative phase measurement) capture with color CCD of Au nanodiscs with 86 nm diameter and 20 nm height on Cr/Poly(methyl methacrylate)/borosilicate glass slide | Medium complexity: • thermal evaporation of Au, Cr • etching • tape-stripping • surface functionalization | Point of darkness at: • $\lambda = (640\text{--}650)$ nm • $\theta \approx 55^\circ$ | Ethylene glycol 1) 2.5% ($n = 1.355$) 2) 5% ($n = 1.360$) 3) 60 kD protein NeutrAvidin (NA) | Relative phase shift from 1) $\approx 170^\circ$ and to 2) $\approx 145^\circ, \approx 25^\circ$ phase shift for 0.005 refractive index difference, 3) Sensitivity 200–275 NA molecules per nanodisc | [18] |
| Single surface and multilayer systems | | | | | |
| $\theta = 45^\circ$ dual-drive symmetric photoelastic modulator ellipsometer with microfluidic system based on Si/PDMS/prism | Medium complexity: • SiO ₂ removal from Si • hydroxylation and amination • microfluidic flow fabrication (lithography) • surface functionalization | Biolayer $\theta_B = 69^\circ$, when the $\theta = 55.07^\circ$ for prism at $\lambda = 650$ nm | Human immunoglobulin IgG in the concentration range of 15–1000 ng mL ⁻¹ ; limit of detection is 15 ng mL | No sensitivity to Ψ . Simulation data: • $\Delta = -2.896 d + 177.583$ for $n = 1.330$ • $\Delta = -2.390 d + 178.013$ for $n = 1.334$ • $\Delta = -2.023 d + 178.300$ for $n = 1.338$ Additional data added from the authors of this work: • $d\Delta \approx 3^\circ$ for 1 nm thickness change • $d\Delta \approx -0.132 - 2.711 d$ • $d\Delta \approx 66 - 50 n$ | [6] |
| SE of Ag/MMA/Ge/Ag on Si | Low complexity: • thermal evaporation of Ag, Ge • spin-coating of MMA • surface functionalization | Point of darkness at: • $\lambda = 708$ nm • $\theta = 65^\circ$ | 1 pM streptavidin with $\approx 11.8 \times 10^5$ M ⁻¹ concentration | $d\Psi \approx 5.9^\circ$ $d\Delta \approx 33^\circ$ | [20] |

be deposited by common vacuum thin film technologies used in semiconductor industries with no need of lithography and etching processes. Moreover, this would be much simpler sensor configuration, where only single wavelength and single incident angle could be used.

2. Modeling

The sensor and optical model for Si substrate with five to six layers is shown in Figure 1. Main ellipsometric formula can be written with the following expressions:

1) Reference samples defined as a clean sensor

$$\tan \Psi_{\text{Ref}} \exp(i\Delta_{\text{Ref}}) = \rho_{\text{Ref}}(\widetilde{N}_0, \widetilde{N}_1, \widetilde{N}_2, \widetilde{N}_3, d_1, d_2, d_3, d_4, d_5, \lambda, \theta) \quad (2)$$

2) Sensor with some ultrathin layer on the top

$$\tan \Psi_L \exp(i\Delta_L) = \rho_L(\widetilde{N}_0, \widetilde{N}_1, \widetilde{N}_2, \widetilde{N}_3, \widetilde{N}_6, d_1, d_2, d_3, d_4, d_5, d_6, \lambda, \theta) \quad (3)$$

where d is the thickness of the film/layer. Each layer is characterized by its own \widetilde{N} function and d , what is indicated with the numbering from 0 to 6. Figure 1 shows an example for the sensor made of five layers on Si, but this formalism can be applied to any other number of layers also on the substrates different from Si. The optical properties of the layer 1 are equal with optical properties of the layer 5, and also the layer 2 and layer 4 optical properties are identical; only thickness is different. Such “fiber” sandwich structure, where $\widetilde{N}_0 > \widetilde{N}_1 > \widetilde{N}_2 > \widetilde{N}_3$, the electric field coupling and enhancement are facilitated.^[28,29] Moreover,

a great increase in phase shift can be obtained, thus providing a sensor with two sensitive parameters—reflectivity and phase.

The zero reflection and phase shift are the functions of wavelength λ , incident angle of light θ , and polarization state of light. This concept can be written and analyzed using main ellipsometry formula (1): 1) phase shift Δ between phases δ_p and δ_s for p and s polarized light, which can reach values equal or near to -180° or $+180^\circ$ or alternatively equal or near to 0° or 360° ; practically it is a situation, when the reflected waves are out of phase; 2) ratio of the complex Fresnel's coefficients \tilde{r}_p and \tilde{r}_s for p and s polarized light reaches zero $\tan = \tilde{r}_p/\tilde{r}_s = 0$, which is the case of perfect absorption of p -polarized light.

Typically, where Ψ reaches minimum or maximum values due to interference phenomena in thin films, the Δ might exhibit abrupt phase jumps. It should be noted that it is not directly possible to use the abrupt Δ jump for sensing, thus the close to zero reflection condition and close to abrupt Δ jump measurements are sufficient for sensing applications.

The variation in Ψ and Δ is calculated as a difference in Ψ and Δ before and after the presence of another 0.1 nm thin layer on the top of the sensor (Figure 1): $d\Psi = \Psi_{\text{Ref}} - \Psi_L$ and $d\Delta = \Delta_{\text{Ref}} - \Delta_L$, where Ψ_{Ref} and Δ_{Ref} are for the clean sensor as a reference, and Ψ_L and Δ_L are in case the sensor has 0.1 nm thin layer on the top. The thin layer is simulated as polymethyl methacrylate (PMMA) material. The thickness of 0.1 nm can be considered thin enough to simulate sensor sensibility because dimension of organic molecules is in the range of 3–20 nm. For example, to reach the difference in Ψ and Δ for the sensor presented in the article of Sreekanth et al.,^[20] for ideal multilayer structure the thickness of polymer layer on the top of the sensor must be at least 0.2–0.3 nm to obtain $\approx 30^\circ$ difference in Δ and at least 20–30 nm thick to reach $\approx 6^\circ$ difference in Ψ . The variation in the thickness is always accompanied with the large variation in Δ . In case of 20–30 nm polymer layer on the sensor, the variation in Δ should reach values up to 150° . Small variations in Δ reported in the work of Sreekanth et al.^[20] probably are related to the biotin layer attached to the surface of the sensor to promote the streptavidin adhesion. The biotin and streptavidin probably have similar (n, k) values, thus reducing the variation in Δ with the presence of streptavidin on the biotin layer.

The multilayer sensor system presented in this article is inspired by analysis and modeling of Ag/MMA/Ge/Ag system.^[20] We found that for this system, for the given thicknesses the greatest variation in $d\Psi$ and $d\Delta$ is in UV region rather than in IR spectral range. This sensor, in principle, is an asymmetric Fabry–Perot configuration with large amount of optical loss Ge thin film thinner than the wavelength of light.^[20,27] The high losses Ge supports the creation of “narrow” spectral zones with minimum values of Ψ and sharp Δ change, lowers total amplitude of Δ , and lowers the variation of $d\Psi$ and $d\Delta$. This argument will be discussed in detail in a separate article. In case of phase sensitive sensor development working in visible spectral range, the low loss semiconductors could be considered to build an effective point of darkness.

On the contrary, as not always it is possible to develop optical sensors working with near UV or IR light, and not always it is convenient to work with oxidizing metals as Ag, other materials are proposed in this work: Ag is substituted with Au, and instead

of high refractive index Ge semiconductor ($n = 5.74$ @ 600 nm), we propose low refractive index semiconductors, such as YHO ($n \approx 2.28$ @ 600 nm) or ZnO_x (1.67 @ 600 nm).^[23] If the thicknesses of Au, YHO or ZnO_x , and SiO_2 are smaller than the wavelength of light, that results in the 1) rise of $d\Psi$ and $d\Delta$ variation, 2) shift of the sensitive region from near UV to the visible range, 3) and in shift of sensitive incidence angles of light from $\approx 70^\circ$ to $\approx 40^\circ$. The alternative multilayer proposed in this article is made of five layers on Si (Figure 1): $\text{Au}(d_1)/\text{YHO}(d_2)/\text{SiO}_2(d_3)/\text{YHO}(d_4)/\text{Au}(d_5)$. Some discussion will be devoted also for the case, where even lower refractive index material with respect to YHO is used, such as ZnO_x . The impact of the thickness $d_1, d_2, d_3, d_4, d_5, d_6$ variation will also be discussed.

In the simulations we use the complex dielectric dispersion curves obtained from WOOLLAM RC2 SE investigations for YHO and ZnO_x .^[28] Thin films developed at the Thin Film Laboratory of ISSP UL. The fabrication process and characteristics of ZnO_x thin films can be found in our reference.^[35] The YHO thin films were fabricated on soda-lime glass using the vacuum PVD coater G500M (Sidra Vacuum, Ltd.). YHO films were deposited by reactive DC magnetron sputtering from Y (purity 99.95%) target in an Ar (99.9999%) and H_2 (99.999%) atmosphere (H_2 to Ar gas flow ratio of 2:3). The sputtering pressure was varied from 3 mTorr up to 20 mTorr. In this work, YHO sputtered at 3 mTorr obtained (n, k) dispersion curves are used (Figure 2) because such films are not completely oxidized and have $k > 0$ in the spectral range from UV to NIR; YHO sputtered at higher pressure exhibit photochromic properties and $k > 0$ only above optical bandgap.

The dispersion curves for Si, SiO_2 , and Au were selected from the WOOLLAM CompleteEASE software optical constant library. The (n, k) wavelength dependence of all materials used in simulations is shown in Figure 2. The simulations are performed using CompleteEASE by modeling the main ellipsometric angles (Ψ, Δ) as a function of incident angle θ and photon energy $E = hc/\lambda$, where h is the Planck's constant and c is the speed of light, and with COMSOL to obtain detailed maps of reflectivity and phase shifts in variation of the sensor thicknesses and incident angles of light to find the best combination of the thicknesses for the highest sensitivity.

The modeling is performed in the spectral range of 1–5 eV or 248–1240 nm with two different steps: 0.02 eV or 1 nm, 0.0028 eV or 0.1 nm, and 0.05 nm. No modeling was performed for steps finer than 0.01 nm to be consistent with spectral resolution of common existing spectroscopic methods (e.g., WOOLLAM RC2 and similar SE wavelength resolution at UV–VIS is ≈ 1.0 nm; Cary 7000 universal measurement spectrophotometer wavelength resolution at UV–VIS < 0.048 nm). The incident angle of light was varied in the range of $(30.00\text{--}75.00)^\circ$ with $2.0^\circ, 0.5^\circ$, and 0.1° steps.

3. Results

The modeling shows that the sensor has quasi-zero reflection in the broad spectral range of 540–350 nm (or 2.3–3.5 eV, Figure 3a) for the following configuration: Si/Au (30 nm)/YHO (12 nm)/ SiO_2 (35 nm)/YHO (15 nm)/Au (6 nm). This configuration gives the greatest variation in Δ . More detailed spectra at $\theta = [30.0^\circ; 50.0^\circ]$

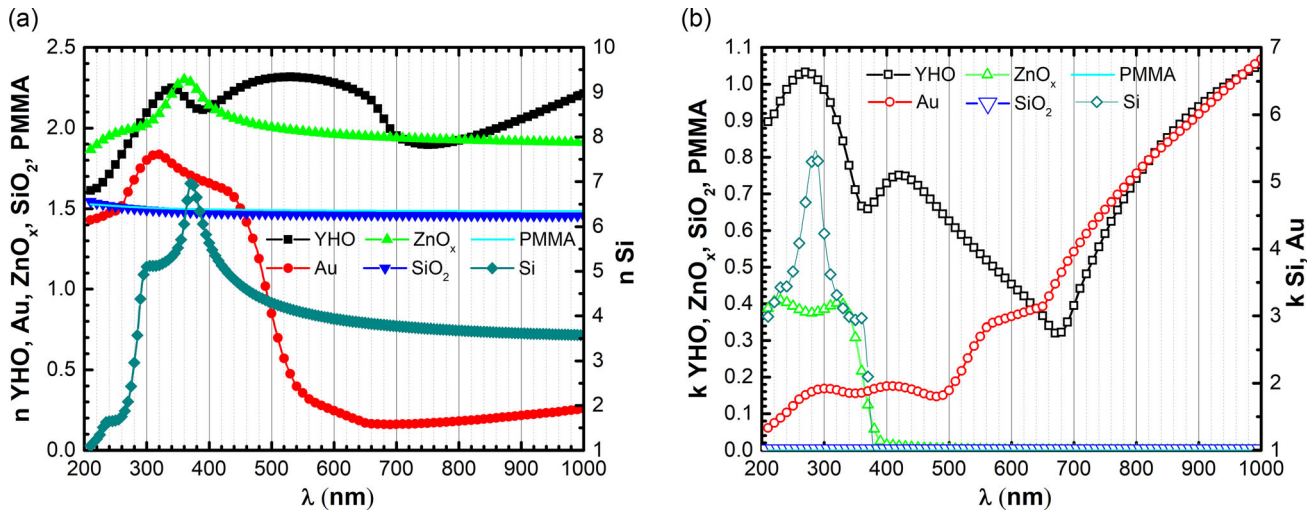


Figure 2. a) Dispersion curves of refractive index n and b) extinction coefficient k used in the modeling.

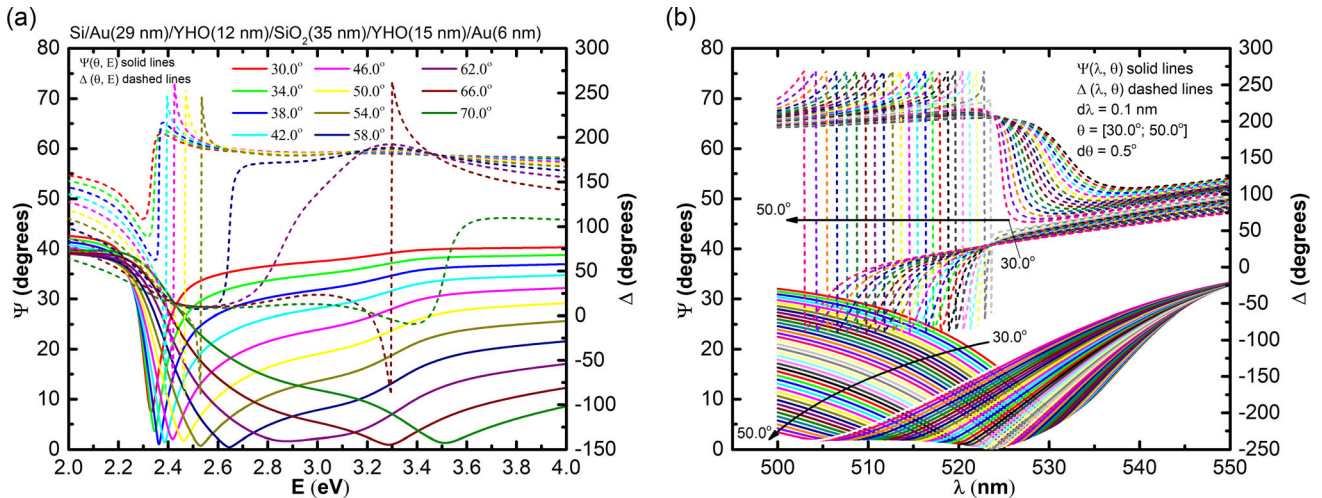


Figure 3. Main ellipsometric angles (Δ , Ψ) as a function of a) photon energy or b) wavelength with a) 0.02 eV and b) 0.1 nm step. The incident angle is varied from 30° up to 70°.

with the 0.5° step are shown in Figure 3b. Sharp Δ shift of about 340° with quasi-zero reflection is observed in the spectral range of ≈ 505 –300 nm. Also, at the shorter wavelengths of UV similar values can be seen (Figure 3a). In case of pure reflectivity measurements, the sensor is sensitive in the visible light spectral range of ≈ 510 –535 nm reaching $d\Psi$ values up to 0.22° and -0.12° , what is of 1) one order more for NIR and 2) approximately two times higher values for UV with respect to the sensors containing Ge.^[20] In case of phase singularities, the largest $d\Delta$ of 225° is observed at $\lambda = 523.7$ nm and at $\theta = 38.9^\circ$ for the spectral scan (Figure 4a) and at $d\Delta = \pm 130^\circ$ for $\theta = [38.7^\circ; 39.0^\circ]$ scan (Figure 4b). These $d\Delta$ values are 2–3 times higher with respect to sensors containing Ge.^[20] A simple Si substrate biosensor^[6] simulation shows that $d\Delta$ is only about 3° in case of 1 nm thin biolayer on the top of Si, and experiment evidenced no sensitivity to Ψ .

The biggest problem of the phase sensitive sensor development is the selection of the proper λ and θ region due to the

abrupt Δ jumps.^[19] Even if very high $d\Delta$ is observed at particular λ and θ , it does not mean it will be possible to measure broad range of different thicknesses d_6 for the layer 6 to be detected. With increase in d_6 , the Δ and $d\Delta$ abrupt jump is shifting toward shorter λ in case of λ scan at fixed θ , and toward smaller θ in case of θ scan at fixed λ (Figure 5). For this reason, λ and θ should be chosen near the point of darkness.

Depending on selected (θ, λ) , it is possible to obtain sensors sensitive 1) only to Ψ , 2) only to Δ , or 3) to both for the variation of d_6 (Figure 6a) and n_6 (Figure 6b). Linear variation of $d\Psi$ and exponential variation of $d\Delta$ can be obtained at $\theta = 40.0^\circ$, $\lambda = 522.5$ nm, where $d\Psi = 0.0630 - 1.1701d_6$ and $d\Delta = 41.0173(1 - \exp(-1.2875d_6))^{0.7544}$. There is very pronounced Ψ sensitivity at $\theta = 30.0^\circ$, $\lambda = 533.5$ nm, with very small Δ variation: $d\Psi = -0.07186 + 2.39133d_6$, and $d\Delta = 0.07829 + 0.10462d_6 + 0.78168d_6^2 - 0.80666d_6^3$. High phase **senility** can be obtained at $\theta = 39.0^\circ$, $\lambda = 524.0$ nm,

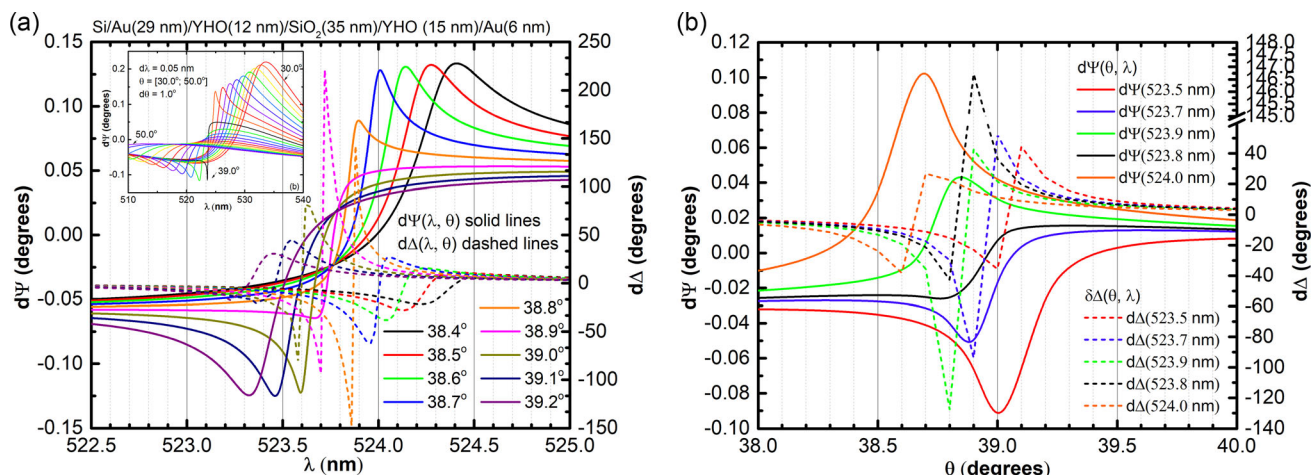


Figure 4. a,b) Two spectral sections and c,d) three incident angle sections. Difference of Δ , Ψ as a function of the a) λ and b) θ ($d\Delta$, $d\Psi$). The λ is varied with the step of 0.05 nm, and θ with the step of 0.1°.

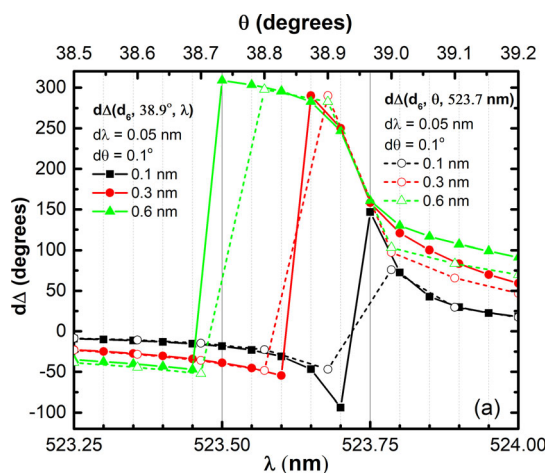


Figure 5. Phase shift difference $d\Delta$ as a function of thickness d_6 (polymer layer on the top of the multilayer sensor) and $(38.9^\circ, \lambda)$, and as a function of $(\theta, 523.7 \text{ nm})$.

where $d\Delta$ reaches 13° and 88° for 0.1 and 1 nm thin layer, respectively. It is almost 30 times higher $d\Delta$ variation with respect to the pure Si,^[6] where n of the solution was about 1.34. In our case n is about 1.5 (see PMMA, in Figure 2). The higher is the difference of the refractive index of the detectable layer respect to the sensor effective n , the higher variation can be observed in (Ψ, Δ) spectra. Thus, for the multilayer sensor the $d\Psi$ and $d\Delta$ could be even larger if we would simulate PMMA with the smaller refractive index.

For biomedical sensor development, it is of high interest to detect the solutions of different concentrations, what can be seen as a variation of refractive index.^[6] Both $d\Psi$ and $d\Delta$ have linear variation with refractive index n_6 (Figure 6b). The fitting parameters of the linear fit are shown in Table 2. The $(40.0^\circ; 522.5 \text{ nm})$ and $(38.0^\circ; 525.0 \text{ nm})$ is a relatively good compromise for double parameter sensing, while at $(39.0^\circ; 524.0 \text{ nm})$ a great sensitivity to phase shift, and at $(38.0^\circ; 525.0 \text{ nm})$ a higher sensitivity to the reflectivity

measurements can be obtained. The slope of $d\Delta(n_6)$ at $(39.0^\circ; 524.0 \text{ nm})$ is of $40n_6$, what is slightly lower with respect to pure Si^[6] (see Table 1), but difference in detectable layer refractive index should be considered as just discussed earlier. Moreover, the aim of this article was to develop sensors sensitive to both reflectivity and phase measurements, what is not the case of pure Si sensor.^[6]

If the thickness d_1 , d_3 , d_4 , or d_5 is increasing or decreasing down to zero, the sensor still has sensitivity in reflection measurements, but loses the sensitivity to the phase variation (Table 3). The increase in the thickness d_2 of YHO permits to shift the spectral region of the (Ψ, Δ) sensitivity.

The sensor can be simplified by removing the layer 4, but the layer 3 thickness must be increased up to 70 nm to keep the sensitivity to Δ : Si/Au (20 nm)/YHO (16 nm)/SiO₂ (70 nm)/Au (10 nm). For such sensor $d\Psi$ reaches -0.15° and $d\Delta$ reaches $\pm 30.0^\circ$ at $\lambda \approx 484.8 \text{ nm}$ and $\theta = 40.5^\circ$. The $d\Psi$ reaches 0.23° at $\lambda \approx 492.5 \text{ nm}$ and $\theta = 35.0^\circ$.

If low (n, k) YHO semiconductor is substituted with the zero-extinction coefficient (at visible range) semiconductor like ZnO_x (Figure 2), the best conditions for the $d\Psi$ and $d\Delta$ sensitivity are at $\lambda \approx 515.8 \text{ nm}$ and $\theta = 32.5^\circ$ with corresponding $d\Psi$ and $d\Delta$ 0.18° and $\pm 55.0^\circ$, respectively (the configuration: Si/Au (60 nm)/ZnO_x (12 nm)/SiO₂(45 nm)/ZnO_x (15 nm)/Au (20 nm)). If the layer 4 is removed (configuration Si/Au (60 nm)/ZnO_x (12 nm)/SiO₂(45 nm)/Au (9 nm)), $d\Psi$ reaches -0.30° and $d\Delta$ reaches $\pm 10.0^\circ$ at $\lambda \approx 471.6 \text{ nm}$ and $\theta = 32.5^\circ$.

Various other simpler sensors can be designed (e.g., Si/Metal/LnkM/Metal, Si/LnkM/Metal, LnkM/Metal/LnkM/Metal, where LnkM is any low (n, k) material such as SiO₂, ZnO_x, PMMA, already reported elsewhere by other researchers^[23,25,26]) to achieve similar or even greater reflectivity sensitivity. However, the phase shift reaching values up to 225° for only 0.1 nm thin detectable layer is unique and showed here for the multilayer of Si/Au (30 nm)/YHO (12 nm)/SiO₂ (35 nm)/YHO (15 nm)/Au (6 nm). The particularity of this configuration is based on low (n, k) YHO semiconductor material, ultrathin thicknesses, and gradual decrease in the refractive index toward SiO₂ layer and accordingly gradual increase in refractive index toward top Au layer for the electric field enhancement.

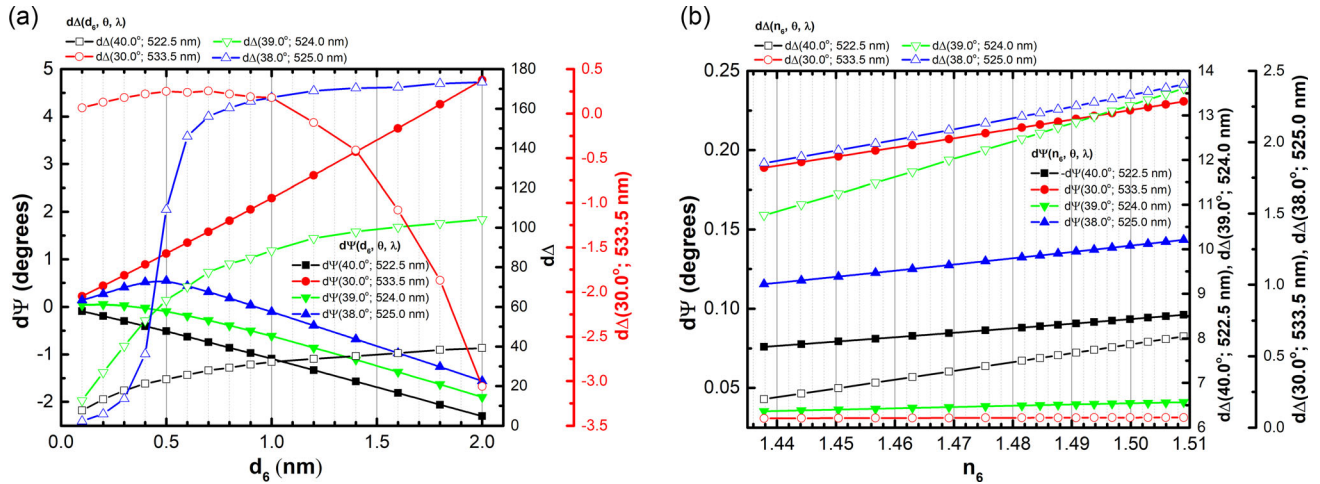


Figure 6. a) The variation of ($d\Psi$, $d\Delta$) as a function of a) d_6 and b) n_6 for 0.1 nm thin d_6 thickness: four examples are given for different combinations of the (θ, λ) .

Table 2. The fitting parameters of the linear fit $d\Psi = A + Bn_6$ and $d\Delta = A + Bn_6$ to the $d\Psi$ and $d\Delta$ functions given in Figure 6b.

| | $d\Psi$ | | $d\Delta$ | |
|-------------------|-----------------------------------|------------------------------------|------------------------------------|-----------------------------------|
| | A | B | A | B |
| (40.0°; 522.5 nm) | 0.33394 ± 0.0014 | $-0.28494 \pm 9.92383 \text{ E-4}$ | -21.8751 ± 0.01641 | 19.8279 ± 0.01109 |
| (30.0°; 533.5 nm) | -0.65848 ± 0.002 | 0.58913 ± 0.00135 | $-0.05249 \pm 7.24999 \text{ E-4}$ | $0.08098 \pm 4.90017 \text{ E-4}$ |
| (39.0°; 524.0 nm) | $-0.08036 \pm 5.7915 \text{ E-4}$ | $0.08042 \pm 3.9144 \text{ E-4}$ | -46.79548 ± 0.19754 | 40.01705 ± 0.13351 |
| (38.0°; 525.0 nm) | -0.45124 ± 0.00155 | 0.39397 ± 0.00105 | -9.34342 ± 0.0694 | 7.78125 ± 0.0469 |

Table 3. The characteristics (behavior) of minimum values of Ψ_{\min} (zero or quasi-zero reflection), Δ shift at corresponding $d\Psi_{\min}$, difference in $d\Psi$ and $d\Delta$ with the variation (increase \uparrow , decrease \downarrow) of d_1, d_2, d_3, d_4, d_5 .

| Ψ_{\min} and $d\Psi$ | | | Δ and $d\Delta$ |
|---------------------------|--------------|--|---|
| d_1 | \uparrow | Ψ_{\min} is \uparrow and slightly shift toward longer λ | $\Delta \uparrow$, $d\Delta \downarrow$ and reaches 0° |
| | \downarrow | Ψ_{\min} is \uparrow and slightly shift toward shorter λ | $\Delta \downarrow$, $d\Delta \downarrow$ and reaches 0° |
| d_2 | \uparrow | $\Psi_{\min} \uparrow$ up at $\approx 5^\circ$ and strongly shift toward longer λ ; for the thickness from 10 to 50 nm the λ of Ψ_{\min} moves between 515 and 660 nm; $d\Psi$ reaches $\approx -0.11^\circ$ and $\approx 0.04^\circ$ | $\Delta \uparrow$ from $\approx 250^\circ$ up to 350° ; $d\Delta \approx \pm 40^\circ$ |
| | \downarrow | Ψ_{\min} is \uparrow and slightly shift toward shorter λ | $\Delta \downarrow$, $d\Delta \downarrow$ and reaches 0° |
| d_3 | \uparrow | Ψ_{\min} is \uparrow and slightly shift toward longer λ | $\Delta \uparrow$, $d\Delta \downarrow$ and reaches 0° |
| | \downarrow | Ψ_{\min} is \uparrow and slightly shift toward shorter λ | $\Delta \uparrow$, $d\Delta \downarrow$ and reaches 0° |
| d_4 | \uparrow | Ψ_{\min} is \uparrow and slightly shift toward longer λ , $d\Psi \approx -0.12^\circ$ | $\Delta \uparrow$, $d\Delta \downarrow$ and reaches 0° |
| | \downarrow | Ψ_{\min} is \uparrow and slightly shift toward shorter λ , $d\Psi \approx +0.12^\circ$ | $\Delta \uparrow$, $d\Delta \downarrow$ and reaches 0° |
| d_5 | \uparrow | Ψ_{\min} is \uparrow and slightly shift toward shorter λ | $\Delta \downarrow$, $d\Delta \downarrow$ and reaches 0° |
| | \downarrow | Ψ_{\min} is \uparrow and slightly shift toward shorter λ , $d\Psi \approx -0.25^\circ$ | Δ maximum values remain the same, $d\Delta \downarrow$ and reaches 0° |

4. Conclusion

High reflection and phase shift sensitivity can be achieved by design of five-layer sensor (Figure 1), where $\tilde{N}_0 > \tilde{N}_1 > \tilde{N}_2 > \tilde{N}_3$, $\tilde{N}_1 = \tilde{N}_5$ and $\tilde{N}_2 = \tilde{N}_4$. The highest variation of Δ up to 225° is observed

at $\lambda = 523.7$ nm and at $\theta = 38.9^\circ$ for the multilayer configuration of Si/Au (30 nm)/YHO (12 nm)/SiO₂ (35 nm)/YHO (15 nm)/Au (6 nm). This sensor has quasi-zero reflection in the broad spectral range of (350–540) nm between $\theta = [30.0^\circ; 70.0^\circ]$. Enhanced double sensing of ($d\Psi$, $d\Delta$) has been observed at $\lambda = 522.5$ nm and

$\theta = 40.0^\circ$, where $(d\Psi, d\Delta)$ varies linearly with the detectable material refractive index change, and $d\Psi$ varies linearly and $d\Delta$ varies exponentially with the detectable material thickness change. The increase in the thickness d_2 of YHO permits to shift the spectral region of the (Ψ, Δ) sensitivity.

Acknowledgements

This research was supported by the Horizon 2020 Project CAMART² under grant agreement No. 739508 and national project "Thin films of rare-earth oxy-hydrates for photochromic applications" FLPP No. LZP-2020/2-0291.

Conflict of Interest

The authors declare no conflict of interest.

Data Availability Statement

Research data are not shared.

Keywords

absorption of light, biomedical sensors, dielectrics, ellipsometry, phase shift, point of darkness, reflectivity, semiconductors

Received: June 30, 2021

Revised: August 2, 2021

Published online:

- [1] *Biosensors Market Size, Share & Trends Analysis Report By Application (Medical, Agriculture, Environment) By Technology (Thermal, Electrochemical, Optical), By End-use, By Region, And Segment Forecasts, 2021-2028*, Report ID: 978-1-68038-321-8, Published Date: April, 2021.
- [2] M. Pirzada, Z. Altintas, *Micromach.* **2020**, *11*, 356.
- [3] P. Damborský, J. Švitel, J. Katrlík, *J. Opt. Biosensors Essays Biochem.* **2016**, *60*, 91.
- [4] T. Nagatsuka, H. Uzawa, D. Tanaka, Y. Oba, Y. Nishida, T. Iwasa, K. Tayama, T. Yoshida, T. Ezaki, Y. Seto, *Sens. Actuators B Chem.* **2017**, *246*, 937.
- [5] G. G. Daaboul, R. S. Vedula, S. Ahn, C.A. Lopez, A. Reddington, E. Ozkumur, M.S. Ünlü, *Biosens. Bioelectr.* **2011**, *26*, 2221.
- [6] K. Li, S. Wang, L. Wang, H. Yu, N. Jing, R. Xue, Z. Wang, *Sensors* **2018**, *18*, 15.
- [7] H. Arwin, *Sens. Actuators A* **2001**, *892*, 43.
- [8] R. M. Ostroff, D. Hopkins, A. Haeberli, W. Baouchi, B. Polisky, *Clin. Chem.* **1999**, *45*, 1659.
- [9] C.-M. Jan, Y.-H. Lee, K.-C. Wu, C.-K. Lee, *Opt. Express* **2011**, *V19*, 5431.
- [10] H. Arwin, *Ellipsometry In Life Science*, Vol. 1, William Andrew Publishing/Springer Verlag, Norwich, NY **2005**, pp. 799–855.
- [11] <https://www.metricon.com/specifications> (accessed: June 2021).
- [12] <https://schaefer-tec.com/en/products/ulvac-high-speed-ellipsometer/> (accessed: June 2021).
- [13] <https://www.phaselabinstrument.com/ipso.html> (accessed: June 2021).
- [14] M. Kim, Z. Jacob, J. Rho, *Light: Sci. Appl.* **2020**, *9*, 130.
- [15] D. E. Aspnes, *Thin. Solid Films* **2014**, *571*, 334.
- [16] H. G. Tompkins, E. A. Irene, *Handbook of Ellipsometry* **2005**, ISBN 978-0-8155-1499-2, William Andrew Inc., 886 pages.
- [17] V. G. Kravets, F. Schedin, R. Jalil, L. Britnell, R. V. Gorbachev, D. Ansell, B. Thackray, K. S. Novoselov, A. K. Geim, A. V. Kabashin, A. N. Grigorenko, *Nat. Mater.* **2013**, *12*, 304.
- [18] M. Svedendahl, R. Verre, M. Kall, *Sci. Appl.* **2014**, *3*, 220.
- [19] H. Song, N. Zhang, J. Duan, Z. Liu, J. Gao, M. H. Singer, D. Ji, A. R. Cheney, X. Zeng, B. Chen, S. Jiang, Q. Gan, *Adv. Opt. Mater.* **2017**, *5*, 1700166.
- [20] K. V. Sreekanth, S. Sreejith, S. Han, A. Mishra, X. Chen, H. Sun, C. T. Lim, R. Singh, *Nat. Comm.* **2018**, *9*, 369.
- [21] S. Ramanathan, F. Capasso, *App. Phys. Lett.* **2012**, *101*, 221101.
- [22] S. R. Amanaganti, M. Ravník, J. Dontabhtuni, *Sci. Rep.* **2020**, *10*, 15599.
- [23] H. Kocer, S. Butun, Z. Li, K. Aydin, *Sci. Rep.* **2014**, *5*, 8157.
- [24] V. G. Kravets, F. Schedin, R. Jalil, L. Britnell, R. V. Gorbachev, D. Ansell, B. Thackray, K. S. Novoselov, A. K. Geim, A. V. Kabashin, A. N. Grigorenko, *Nat. Mater.* **2013**, *V12*, 304.
- [25] J.-B. You, W.-J. Lee, D. Won, K. Yu, *Opt. Express* **2014**, *V22*, 8339.
- [26] S. Shu, Z. Li, Y. Y. Li, *Opt. Express* **2013**, *V21*, 25307.
- [27] M. A. Kats, R. Blanchard, P. Genevet, F. Capasso, *Nat. Mater.* **2013**, *12*, 20.
- [28] A.A. Khosroabadi, P. Gangopadhyay, S. Hernandez, K. Kim, N. Peyghambarian, R. A. Norwood, *Materials* **2015**, *8*, 5028.
- [29] S. Singh, S. K. Mishra, B. D. Gupta, *Sens. Actuators A* **2013**, *193*, 136.
- [30] Y. Li, B. An, S. Jiang, J. Gao, Y. Chen, S. Pan, *Opt. Express* **2015**, *23*, 17607.
- [31] Y. Yao, Z. Liao, Z. Liu, X. Liu, J. Zhou, G. Liu, Z. Yi, J. Wang, *J. Phys. D: Appl. Phys.* **2021**, *54*, 113002.
- [32] Z. Liu, G. Liu, X. Liu, G. Fu, *Nanotechnology* **2020**, *31*, 115208.
- [33] Y. Yang, I. I. Kravchenko, D. P. Briggs, J. Valentine, *arXiv:1405.3901*, **2014**.
- [34] A. Shalabney, I. Abdulhalim, *Laser Photon. Rev.* **2011**, *5*, 571.
- [35] M. Zubkins, J. Gabrusenoks, G. Chikvaidze, I. Aulika, J. Butikova, R. Kalendarev, L. Bikse, *J. Appl. Phys.* **2020**, *128*, 215303.